J Electroceram (2012) 29:56–61
DOI 10.1007/s10832-012-9738-z

Interface and ionic interdiffusion in cofired dielectrics/ferrite layer composites

Xiangchun Liu

Received: 5 December 2011 / Accepted: 30 April 2012 / Published online: 13 May 2012

Abstract Zinc-magnesium titanate dielectrics/nickel-zinc-copper ferrite layer composites were prepared. An interlayer was designed to relax the interfacial stress because of the mismatch shrinkage between dielectric and ferrite. And as the results, zero camber and crack-free dielectric/interlayer/ferrite composite samples were obtained and the interface was continuous with no delamination. The cofiring interface and ionic interdiffusion between the constituents were investigated. The interdiffusion of the composite can be regarded as the semi-infinite diffusion-couple model and based on this diffusion model, the numerical simulation for the ionic composition distribution was carried out by computer, which was in agreement with the experimental results. The activation energies for the Ti^{4+}, Ni^{2+}, and Fe^{3+} were determined respectively. The difference between apparent activation energies was discussed in this article. The layer composite sintered at 930°C exhibited the dielectric properties: ε_r=18.2, $\tan\delta=3.01\times10^{-3}$. Due to their low firing characteristics and realizable co-firing compatibility, the layer composites can serve as the promising medium materials in the multilayer LC filter.

Keywords Cofired · Sintering · Layered structures · Interfaces · Ionic diffusion

1 Introduction

In recent decades, development of low temperature co-fired ceramic technology (LTCC) has been geared up due to the huge demand of miniaturisation of electronic components. New materials are being developed for extending the demand of wide range of dielectric properties of LTCC, minimization of shrinkage, cambering of LTCC, high quality of conductors and patterning etc. [1]. Multilayer chip LC filters have been developed as a type of promising miniaturisation of electronic components. They are made by stacking ferrite layers and dielectric layers with internal electrode pastes, and then cofired. The sintering temperature of ferrite and dielectrics must be below 900°C to ensure their cofiring with Ag internal electrode [2]. The properties of devices depend on the properties of the sintered ferrites, dielectrics and the quality of the interface. On the one hand, interfacial diffusion is inevitable, and this process can affect properties near the interface. On the other hand, the mismatch in sintering kinetics between different kinds of ceramics may cause residual stresses or cracks. Therefore, the matching and compatibility during low-temperature co-firing process is the key to achieve multilayer chip composites [3].

Zinc titanate ($ZnTiO_3$) is a promising candidate for low temperature sintering dielectrics, because it can be sintered at 1100°C without sintering aids and can be sintered at temperature <900°C with B_2O_3 glass. But this phase will decompose as the sintering temperature is above 900°C [4, 5]. The previous studies have shown that the phase stability of $ZnTiO_3$ was greatly enhanced due to the magnesium substitution, and the hexagonal phase stability region extended from 900 to 1150°C [6], which provided a significant benefit to develop the LTCC $ZnTiO_3$-based ceramics. And the sintering temperature of hexagonal ilmenite-type $(Zn_{0.7}Mg_{0.3})TiO_3$ (Abbreviated to ZMT3) dielectric ceramics were lowered from 1200°C to 875°C successfully by a semichemical rout and 1.0 wt% V_2O_5 additions. Nickel-zinc-copper ferrite (Abbreviated to NZC), which has excellent magnetic permeability and can be sintered at low

X. Liu (✉)
Department of Materials Science and Engineering, Xi'an University of Science and Technology,
Xi'an 710054, Peoples Republic of China
e-mail: liuxc@126.com

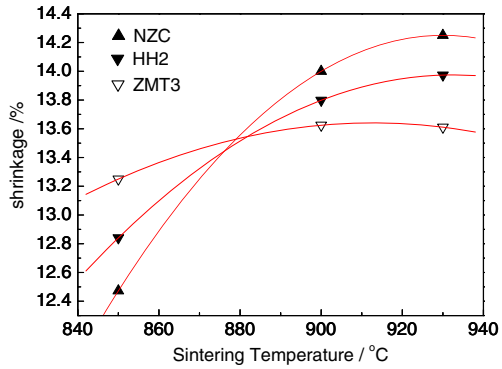

Fig. 1 Radial shrinkage curve of HH2, ZMT3 and NZC

temperature, is an important material using for producing low temperature sintered multilayer chip inductor (MLCI) [7–9]. They are promising materials for the multilayer chip LC filters.

In our previous work, the multilayer composites were prepared by cofiring ZMT3 dielectrics and NZC ferrite at 900°C. But the camber was observed in ZMT3 dielectrics/NZC ferrite composites because of the mismatch shrinkage at the temperature range from 875°C to 930°C. So in present paper, the interlayer was designed to relax the interfacial stress resulting from the shrinkage difference between ZMT3 and NZC. The cofiring interface and kinetics of ionic interdiffusion between constituents were investigated.

2 Experimental procedure

The firstly, NZC ferrite and ZMT3 powders were synthesized by solid-state reaction method combined with a chemical processing.

$(Zn_{1-x}Mg_x)TiO_3$ (x=0 to x=0.5) system was prepared using a semichemical rout with A.R zinc hydroxide carbonate ($Zn_5(CO_3)_2{\cdot}(OH)_6$), A.R magnesium hydroxide carbonate ($Mg(OH)_2{\cdot}4\ MgCO_3{\cdot}6\ H_2O$) and anatase ($TiO_2$, 10~30 nm). The carbonates were heat-treated at 350°C and 540°C for 2 h in air to obtain nanopowder ZnO (10~30 nm) and MgO (20~50 nm) with high activation energy as starting materials, respectively. X-ray diffractometry (XRD) confirmed that pure phase ZnO and MgO were obtained. Anatase nanopowder was mixed with ZnO, MgO and dispersant, according to the composition of $(Zn_{0.7}Mg_{0.3})TiO_3$, using planetary milling with zirconia balls in ethanol for 24 h. The mixture was dried and then calcined at 750°C for 2 h. The resultant powders were the ZMT3 starting material.

Ninety-nine percent pure reagent-grade NiO, Fe_2O_3, CuO and high active ZnO nanopowder, according to the composition of $(Ni_{0.8}Cu_{0.12}Zn_{0.12})Fe_{1.96}O_4$, were weighted and mixed for 12 h in a planetary ball mill. The mixtures were calcined (720°C for 4 h) as NZC starting material.

Then the ZMT3 starting material and NZC starting material were mixed in weight ratio 1: 1. The resultant mixed powders (named HH2) acted as interlayer to relax the interfacial stress resulting from the shrinkage difference between ZMT3 and NZC.

Next, the sintering additives (V_2O_5 for ZMT3, Bi_2O_3 for NZC), solvent, dispersant, binder, and plasticizer were mixed into the ZMT3 starting material, HH2 mixed powders and NZC starting material respectively and milled for 48 h respectively to prepare the slurries.

After being sifted out and eliminated the air bubbles, the slurries were dried and granulated. Then the multi-layer samples were assembled by stacking granulated powders of NZC, HH2 and ZMT3 in the order of NZC, HH2, ZMT3 and were pressed (60 MPa) at 60°C for 10 min.

At last, the binder was burnt out before sintered by heating up very slowly to 350°C, and kept 6 h at this temperature. The samples were sintered at 900~930°C in air for 4 h.

The sintered densities were measured by the Archimedes method. Interfacial diffusion was examined by scanning electron microscopy (SEM, JEOL JSM-5800, Japan) and energy dispersive X-ray spectroscopy (EDS). The crystalline structure of the samples was investigated using XRD (X' Pert MPD PRO, Holland).

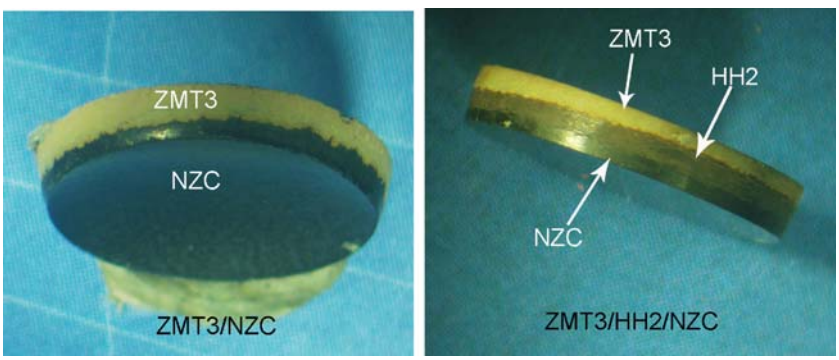

(a) (b)

Fig. 2 Macrographs of ZMT3/NZC and ZMT3/HH2/NZC composite

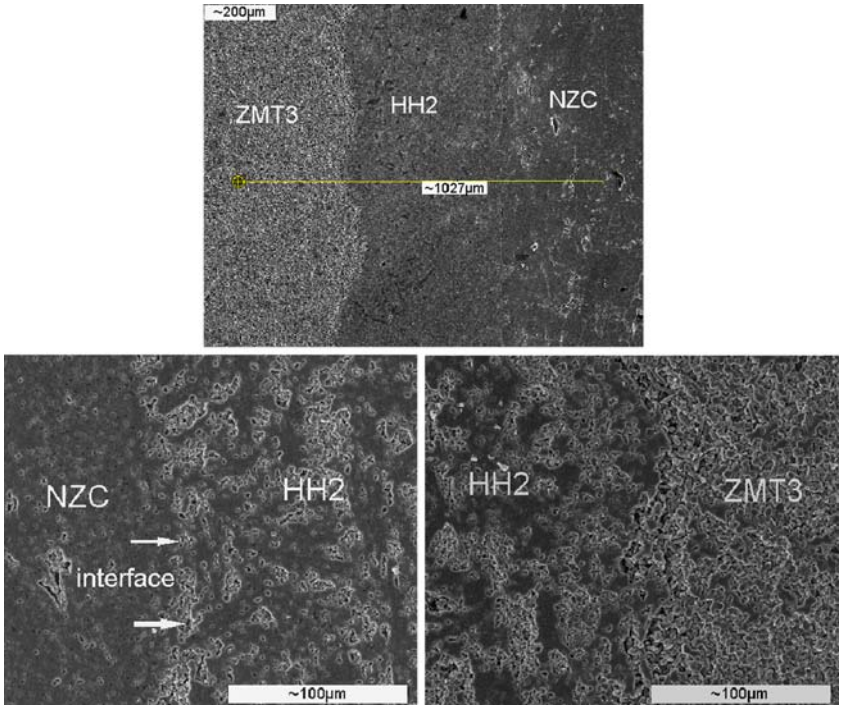

Fig. 3 SEM micrographs of the interfacial structures of ZMT3/HH2/NZC composite

3 Results and discussion

Figure 1 show the radial shrinkage curves of HH2, ZMT3 and NZC. It can be seen that the radial shrinkage of NZC is higher than ZMT3 at the sintering temperature of 900°C. And the mismatch of shrinkage is obvious, as the result, the camber was found in the double-layer ZMT3/NZC composites, as shown in Fig. 2(a). To solve this problem, the radial shrinkage of HH2 was investigated. The results show the radial shrinkage of HH2 is always between that of ZMT3 and NZC (Fig. 1). It is deduced that HH2 may relax the mismatch of shrinkage between ZMT3 and NZC. The experimental results are in agreement with above speculation, which can be seen from Fig. 2(b), zero camber and crack-free ZMT3/HH2/NZC composite sample was obtained.

SEM micrographs of the interfacial microstructure of ZMT3/HH2/NZC composite sintered at 900°C for 4 h are shown in Fig. 3. It can be seen that the interface is continuous with no delamination. An exaggerated grain growth can be observed nearby the interface of the samples and a few pores come into being in the side of ZMT3, which may be attributed to the interfacial phase transition and ionic interdiffusion.

To study the interfacial phase transition and the distribution curves of the characteristic X-ray intensities for the interfacial main element, the XRD and EDS analysis were done and the Figs. 4 and 5 show the results respectively. In Fig. 4, the XRD patterns of ZMT3, HH2 and NZC show the phase structure of ZMT3 powders, HH2 powders and NZC powders sintered at 900°C, respectively. The fracture face pattern represents the cross section of cofired samples at 900°C. From Fig. 4, it can be seen that small of the rutile phase TiO_2 come into being in HH2 powders, but the main phase is the cubic spinel phase. This result shows that the hexagonal ilmenite-type $(Zn_{0.7}Mg_{0.3})TiO_3$ decomposed to $(Zn_{0.7}Mg_{0.3})_2TiO_4$ and TiO_2 when ZMT3 powders and NZC powders are well mixed, but the $(Zn_{0.7}Mg_{0.3})_2TiO_4$ was not be detected. Carefully analyzing the XRD pattern of HH2, it is found that the spinel-type phase composition formed the main phase, which is neither spinel NZC nor spinel $(Zn_{0.7}Mg_{0.3})_2TiO_4$. The d-spacing values of NZC, HH2 and $(Zn_{0.7}Mg_{0.3})_2TiO_4$ are shown in Table 1. The d-spacing values of HH2 are found close to NZC and $(Zn_{0.7}Mg_{0.3})_2TiO_4$. So it can be concluded that the new phase in HH2 is spinel-type solid solution of NZC and $(Zn_{0.7}Mg_{0.3})_2TiO_4$. The exciting thing is that the rutile phase TiO_2 was not be found in the fracture face pattern. The main phase is still the cubic NZC phase and ZMT3 phase. This

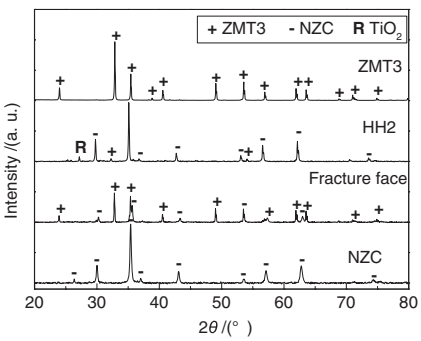

Fig. 4 XRD patterns of ZMT3, NZC, HH2, cross section of cofired samples

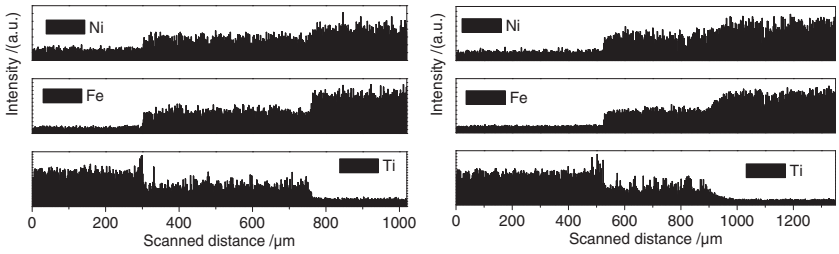

Fig. 5 Concentration distribution curves of the diffusion ions in ZMT3/HH2/NZC diffusion system, a 900°C/4 h, b 930°C/4 h

phenomenon shows that the decomposition of ZMT3 may be very weak so that they can not be detected by XRD. The proper interfacial reactions occurred at the interface can strengthen combinations between ferrite layers and dielectric layers.

The distribution curves of the characteristic X-ray intensities for the ions are shown in Fig. 5. It shows that the ionic diffusion happened across the interface. For Ti^{4+}, Ni^{2+}, and Fe^{3+}, it is revealed that there are three platforms located in a scanning curve from left to right, and each platform is connected by a slope area, as shown in Fig. 6(a). In such platform and slope model, each two adjacent platform and the slope connecting them compose a diffusion couple. The three platforms stand for the ionic concentration in dielectric ZMT3, interlayer HH2 and ferrite NZC, respectively. The slope area is the ionic interdiffusion area between two platforms. Different ions have different thickness of interdiffusion layers. The thickness of the interdiffusion layers was determined by electron probe microbeam analysis.

Because the thickness of the interdiffusion layers is thinner than that of laminated components, the interdiffusion in each diffusion couple can be regarded as semi-infinite diffusion model [10–12] and numerically simulated by computer, the ionic interdiffusion in the couple could be regarded as the interdiffusion in a pair of semi-infinite solids. Semi-infinite diffusion-couple model is shown in Fig. 6(b), and the initial concentrations in diffusion-couple are defined as C_0 and C_s. The ionic diffusion follows Fick's second law, which is expressed in the form of

$$\frac{\partial C}{\partial t} = \frac{\partial}{\partial x}\left(D\frac{\partial C}{\partial x}\right) \tag{1}$$

If the diffusion coefficient D is independent of the position, Eq. 1 simplifies to

$$\frac{\partial C}{\partial t} = D\frac{\partial^2 C}{\partial x^2} \tag{2}$$

It is assumed that the initial concentration distribution is simply stated as

$$\begin{aligned} &C = C_0, x > 0, t = 0 \\ &C = C_s, x < 0, t = 0 \end{aligned} \quad (C_s > C_0) \tag{3}$$

Where C is the ionic concentration, x is the diffusion distance from the interface to the layers, and t is the diffusion time. The solution to Eq. 2 can be yielded by the application of the above boundary conditions in the following manner: imagine the region of $x>0$ is composed of n slices, each with $\Delta\lambda$ thickness and unit cross-sectional area. For each slice, the diffusion solution can be given by thin film solution. If the interactions between the adjacent slices during the diffusion process are neglected, the actual diffusion solution can be obtained by the overlapping the diffusion solution of each thin slice, which is expressed as [13]

$$C(x,t) = C_0 + \frac{C_s - C_o}{2\sqrt{\pi Dt}}\sum_{i=1}^{n}\Delta\lambda_i \exp\left[-\frac{(x-\lambda_i)^2}{4Dt}\right] \tag{4}$$

Where $c(x, t)$ represents the concentration, $\lambda_i$is the distance from the centre of the ith slice to the plane of $x>0$. When the number of the slices n goes to infinity, $\Delta\lambda_i \to 0$. Equation 6 can be written by an integral form, that is

$$C(x,t) = C_0 + \frac{C_s - C_o}{2\sqrt{\pi Dt}}\int_0^{\infty}\exp\left[-\frac{(x-\lambda)^2}{4Dt}\right]\mathrm{d}\lambda \tag{5}$$

Setting $\frac{(x-\lambda)}{2\sqrt{Dt}} = \varepsilon$, Eq. 5 can be rewritten as

$$C(x,t) = C_0 + \frac{C_s - C_o}{2\sqrt{\pi Dt}}\int_0^{\frac{x}{2\sqrt{Dt}}}\exp\left[-\varepsilon^2\right]\mathrm{d}\lambda \tag{6}$$

And introducing the Gaussian error function

$$erf(z) = \frac{2}{\sqrt{\pi}}\int_0^z \exp(-\varepsilon^2)\mathrm{d}\varepsilon \tag{7}$$

Table 1 d-spacing of NZC, HH2 and $(Zn_{0.7}Mg_{0.3})_2TiO_4$

Composition	Crystal structure	d-spacing [Å]				
NZC	spinel	2.97733	2.53450	1.70793	1.61325	1.48004
HH2	spinel	3.00814	2.56115	1.72851	1.62900	1.49547
$(Zn_{0.7}Mg_{0.3})_2TiO_4$	spinel	2.9929	2.5502	1.7271	1.6298	1.4950

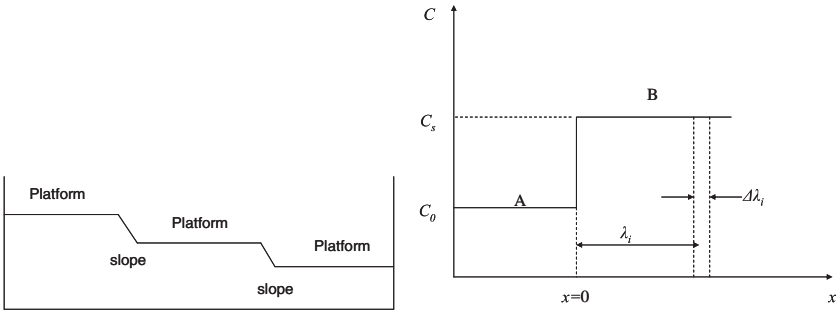

Fig. 6 Schematic diagram of the platform and slope model (**a**) and the initial concent ration distribution for a certain diffusion ion in the A/B semi-infinite diffusion couple (**b**)

Equation 6 can be rewritten as

$$C(x,t) = C_0 + \frac{C_s - C_0}{2}\left[1 + erf\left(\frac{x}{2\sqrt{Dt}}\right)\right] \quad (8)$$

If the boundary conditions are just opposite to that described by Eq. 3, for example, are given by:

$$\begin{aligned} &C = C_0, x > 0, t = 0 \\ &C = C_s, x < 0, t = 0 \end{aligned} \quad (C_s > C_0) \quad (9)$$

then the concentration function $C(x, t)$ transform to:

$$C(x,t) = C_0 + \frac{C_s - C_0}{2}\left[1 - erf\left(\frac{x}{2\sqrt{Dt}}\right)\right] \quad (10)$$

$C(x, t)$ and the ionic diffusion coefficient can be calculated by Eqs. 8 and 10.

From Eqs. 8 and 10, When the $C(x, t)$ is close to C_0, the value of $erf\left(\frac{x}{2\sqrt{Dt}}\right) = 1$, then the parameter $\frac{x}{2\sqrt{Dt}} = 2.80$ determined from error function table. The diffusion coefficient D of Ti^{4+}, Ni^{2+}, and Fe^{3+} ions can be estimated, and the results are given in Table 2. In general, the variety of diffusion coefficient is related to ionic radii, valence, and diffusion circumstances. The diffusion coefficient of Ti^{4+} is bigger than Ni^{4+} and Fe^{3+} in two diffusion couples ZMT3/HH2 and HH2/NZC, which maybe the main reason for the pores in the interface of ZMT3/HH2. It can be seen from Table 2 that the diffusion coefficient varied from sintering temperature, which follows Eq. 11 [11]

$$D = D_0 \exp\left(-\frac{Q_d}{RT}\right) \quad (11)$$

The activation energies for Ti^{4+}, Ni^{2+}, and Fe^{3+} ions are determined from Eq. 11. The activation energies of Ti^{4+}, Ni^{2+}, and Fe^{3+} ions are presented in Table 2. The sequence of activation energies of Ti^{4+}, Ni^{2+}, and Fe^{3+} ions is shown Q_d (Ni^{2+})>Q_d (Ti^{4+})>Q_d (Fe^{3+}) in ZMT3/HH2 diffusion couple and in HH2/NZC diffusion couple, which reveals that the ions with smaller valence is more easy to diffuse in ZMT3/HH2 and HH2/NZC diffusion couples.

The spinel structure has peculiar type of cation distribution among the tetrahedral (Td) and octahedral (Oh) sites of the coordinated oxygen. For a binary oxidic spinel containing divalent A cations and trivalent B cations, two extreme distributions of cations between the Oh and Td sites available are possible: the 'normal' $A[B_2]O_4$ and the 'inverse' $A[AB]O_4$; in each case the ions in the Oh sites are in square brackets. In ternary spinel systems Fe^{3+} ions can be easily shifted between Oh and Td sites by stoichiometrically varying the concentrations of other cations. For NZC ferrite spinel, only zinc will remain in Td site and both nickel and copper can be interchanged with Fe (Oh) sites. The ions meant to occupy Td site need not present exclusively in Td site and it can exchange with Oh site and such a phenomenon results inverse spinel [14]. The same thing can be occurred in $(Zn_{0.7}Mg_{0.3})_2TiO_4$ spinel, Ti^{4+} ions can be easily shifted between Oh and Td sites by stoichiometrically varying the concentrations of other cations. These interchangings may promote the diffusions of Ti^{4+} and Fe^{3+} and these inversions maybe related to the low activation energies of Ti^{4+} and Fe^{3+} ions. The black colour at both the interfaces (HH2-ZMT and NZC-HH2) in SEM images shown in Fig. 3 suggests such inversion is a possibility. But

Table 2 Properties of the diffusion ions

Ions	Ionic radius/nm	Activation energy Q_d /kJ•mol^{-1}		Diffusion coefficient, D /×10^{-16} m^{2}s^{-1}			
		ZMT3/HH2	HH2/NZC	ZMT3/HH2		HH2/NZC	
				900°C	930°C	900°C	930°C
Ti^{4+}	0.68	403.1	590.5	87.4	245	914	4140
Fe^{3+}	0.64	244.4	548.7	74.5	139	434	2280
Ni^{2+}	0.69	497.6	712.3	2.21	7.91	540	3350

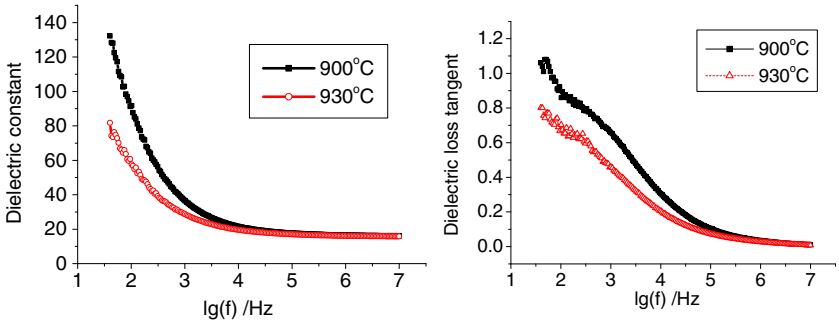

Fig. 7 Dielectric properties of ZMT3/HH2/NZC co-firing samples

these speculations need to be determined by systematical experiments in the future researches.

Figure 7 show the dielectric properties of ZMT3/HH2/NZC cofired composite. It shows a decreasing tendency of all the dielectric constants with increasing measuring frequency. Even at a high frequency, the ε_r value of co-firing samples is presumed to be about 18~20. Similarly, the dielectric loss tangent of co-firing samples decreased gradually with frequency increasing. ZMT3/HH2/NZC layer composite sintered at 930°C exhibited the dielectric properties: ε_r=18.2, tanδ=3.01×10^{-3}. Moreover, much smaller tanδ value at a high frequency can be presumed from the decreasing tendency of tanδ with the increasing value of measuring frequency.

4 Conclusions

The layer composite were prepared by cofiring ZMT3 dielectrics and NiCuZn ferrite. The HH2 interlayer was designed to relax the interfacial stress resulted from the shrinkage difference between dielectric and ferrite. The result show that zero camber and crack-free ZMT3/HH2/NZC composite samples is obtained and the interface was continuous with no delamination. The cofiring interface and ionic interdiffusion between constituents were investigated. The distribution curves of the characteristic X-ray intensities for the ions shows that the ionic diffusion happened across the interface and a semi-infinite diffusion model can be used to characterize ionic interdiffusion between constituents. The numerical simulation for the ionic composition distribution was carried out by computer, which was in agreement with the experimental results. ZMT3/HH2/NZC layer composite sintered at 930°C exhibited the dielectric properties: ε_r=18.2, tanδ=3.01×10^{-3}. Due to their low firing characteristics and realizable co-firing compatibility, the layer composites can serve as the promising medium materials in the multilayer LC filter.

Acknowledgments The work was supported by Doctoral Fund of Ministry of Education of China (20096121120004), Natural Science Foundation of Shaanxi Province under Grant (SJ08ZT05-7), and Scientific Research Program Funded by Shaanxi Provincial Education Department (11JK0821).

References

1. F. Gao, S.B. Qu, Z.P. Yang, C.S. Tian, J. Mater. Sci. Lett. **21**, 15 (2002)
2. F. Gao, J.J. Liu, R.Z. Hong, Z. Li, C.S. Tian, Ceram. Int. **35**, 2687 (2009)
3. M.S. Kim, S. Jeon, D.S. Lee, S.J. Jeong, J.S. Song, J. Electroceram. **23**, 372 (2009)
4. H.T. Kim, S.H. Kim, S. Nahm, J.D. Byun, J. Am. Ceram. Soc. **82** (11), 3043 (1999)
5. A. Chaouchi, S. Marinel, M. Aliouat, S. Astorg, J. Eur. Ceram. Soc. **27**, 2561 (2007)
6. X.C. Liu, F. Gao, L.L. Zhao, C.S. Tian, J. Alloys Compd. **436**, 285 (2007)
7. A. Barba, C. Clausell, J.C. Jarque, M. Monzó, J. Eur. Ceram. Soc. **31**(12), 2119 (2011)
8. Y. Shen, Z. Yue, M. Li, C.W. Nan, J. Electroceram. **21**, 385 (2008)
9. P. Guzdek, J. Kulawik, K. Zaraska, A. Bieńkowski, J. Magn. Magn. Mater. **322**, 2897 (2010)
10. F. Gao, Z.P. Yang, Y.D. Hou, C.S. Tian, J. Mater. Sci. **38**, 1523 (2003)
11. D. William and Jr. Callister, Fundamentals of materials science and engineering, Fifth Edition (Gravure). (John Wiley & Sons, INC., 2008), pp. 132–133.
12. X.C. Liu, F. Gao, C.S. Tian, Solid State Sci. **10**(2), 211 (2008)
13. X. Zhu, J. Xu, Z. Meng, J. Mater. Sci. Lett. **33**, 1023 (1998)
14. K. Sreekumar, T. Mathew, B.M. Devassy, R. Rajgopal, R. Vetrivel, B.S. Rao, Appl. Catal. A **205**, 11 (2001)